Biological arsenite oxidation on iron-based adsorbents in groundwater filters

Kruisdijk, Emiel; Goedhart, Roos; van Halem, Doris

DOI
10.1016/j.watres.2024.122128

Publication date
2024

Document Version
Final published version

Published in
Water Research

Water Research 262 (2024) 122128

Contents lists available at ScienceDirect

Water Research

journal homepage: www.elsevier.com/locate/watres

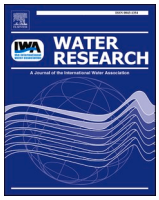

Biological arsenite oxidation on iron-based adsorbents in groundwater filters

Emiel Kruisdijk *, Roos Goedhart, Doris van Halem

Delft University of Technology, Faculty of Civil Engineering and Geosciences, Department of Water Management, Stevinweg 1, 2628 CN Delft, the Netherlands

ARTICLE INFO

Keywords:
Arsenic
Adsorption
Oxidation
Kinetics
Granular ferric hydroxid

ABSTRACT

Iron-based adsorbents are commonly used to remove arsenic (As) from water for drinking water purposes. Here, we study the role of biological As(III) oxidation on iron-based adsorbents in filters and its effect on overall As uptake. A lab-scale filter with iron oxide coated sand (IOCS), a commonly used adsorbent, was operated with water containing As(III) and As(V), while water samples were taken periodically over its height. As(III) oxidation initiated after approximately 10 days and increased to a first order rate constant of 0.09 s^{-1} after 57 days resulting in full oxidation of As(III) in <50 s. Consequently, the filter shifted from an As(III) to an As(V) adsorbing filter. Oxidation was not observed after inhibiting the microbial activity using sodium azide confirming its biogenic nature. This implies that As(III) oxidizing biomass can grow on iron-based adsorbents in water filters without requiring inoculation. As the experimental conditions were similar to full-scale As treatment plants, we believe that biological As(III) oxidation is widely overlooked in these systems. Occurrence of biological oxidation is, however, beneficial for removal, as at pH <8 the adsorption capacity for As(V) can be up to 10-fold higher than for As(III). With these new insights, arsenic treatment using iron-based adsorbents can be further optimized. We suggest a more robust new design with a biological active As(III) oxidizing top layer and an As(V) adsorbing bottom layer.

1. Introduction

Arsenic (As) is found in groundwaters around the world affecting the health of humans and wildlife. It is classified as a human carcinogenic substance (IARC, 2004), which increases the risk for skin lesions and cancers. Podgorski and Berg (2020) estimated that 94 to 220 million people drink or use groundwater with As concentrations exceeding the World Health Organization guideline of 10 μg/L (WHO, 1993). It is generally observed in two redox states, as arsenite (As(III) and arsenate (As(V)). As(III) is the reduced form, and exists as oxyanion [H_3AsO_3] in natural waters at circumneutral pH, while arsenate is the oxidized form found as [$H_2AsO_4^-$ or $HAsO_4^{2-}$]. The reduced form, As(III), is most commonly found in anaerobic groundwaters.

Iron-based adsorbents represent a highly effective method to remove As from water (Banerjee et al., 2008; Driehaus et al., 1998; Sperlich et al., 2005). They are environmentally friendly, highly abundant, and are, therefore, commonly used in wastewater and drinking water treatment (Hao et al., 2018). Oxidation of As(III) to As(V) before treatment is often desired, as the negatively charged As(V) is more efficiently removed via adsorption (Bissen and Frimmel, 2003). Full oxidation with O_2 takes tens of days (Kim and Nriagu, 2000). Therefore, to accelerate this process, chemical oxidants such as, ozone, chlorine, or permanganate are applied, but these oxidation pathways are more costly, need extra chemicals, and increase the risk of unwanted by-products (Miklos et al., 2018). Since the last decade, interest increased in another oxidation pathway: biological As(III) oxidation. Biological As(III) oxidation has already been studied and observed in lab-scale drinking water filters (Crognale et al., 2019; Gude et al., 2018), and bioreactors (Kamei-Ishikawa et al., 2017; Li et al., 2016; Wan et al., 2010). The bioreactors were inoculated with As-oxidizing bacteria, while in rapid sand filters biological As(III) oxidation established without any inoculation. To our knowledge, biological As(III) oxidation on iron-based adsorbents has not yet been studied. The latest review articles on iron-based adsorbents highlight the importance of As(III) oxidation for efficient removal, but only focus on chemical oxidation (Hao et al., 2018; Mohan and Pittman, 2007; Siddiqui and Chaudhry, 2017; Weerasundara et al., 2021).

Gude et al. (2018) showed that biological As(III) oxidation started

* Corresponding author.
E-mail address: e.kruisdijk@tudelft.nl (E. Kruisdijk).

https://doi.org/10.1016/j.watres.2024.122128
Received 12 April 2024; Received in revised form 12 July 2024; Accepted 20 July 2024
Available online 22 July 2024

after one week and really accelerated after two weeks without inoculation on virgin sand in a column study. This and the common occurrence of As(III) oxidizing bacteria in aquatic environments (Crognale et al., 2017), indicate that As(III) oxidizing bacteria are omnipresent. We therefore expect that As(III) oxidizing bacteria can also grow on iron-based adsorbents in water filters. Until now, research on iron-based adsorbents is mostly performed using batch or column experiments, which most often did not take longer than a couple of days (Banerjee et al., 2008; Driehaus et al., 1998; Gupta et al., 2005; Hsu et al., 2008; Mähler and Persson, 2013; Sperlich et al., 2005; Thirunavukkarasu et al., 2003). This could be the reason that As(III) oxidation is never observed, as the duration of these experiments were likely too short for the growth of As-oxidizing bacteria. Driehaus (2002) and Petrusevski et al. (2007) studied full-scale treatment plants in which As was removed by granular ferric hydroxide and iron oxide coated sand, respectively. The lifetime of the media was minimally a year, which we assume is more than enough for the growth of As-oxidizing bacteria, but their presence was never studied.

Based on this information, we hypothesize that biological As(III) oxidation (pH<6.94: $H_3AsO_3+H_2O \rightarrow H_2AsO_4^- +3H^+ +2e^-$, pH >6.94: $H_3AsO_3+H_2O \rightarrow HAsO_4^{2-} +4H^+ +2e^-$) is commonly occurring when treating water for As using iron-based adsorbents. This novel perspective could be of great value for science and practice, as this would imply that treatment with iron-based adsorbents is working differently than understood until now. Based on this knowledge, treatment with iron-based adsorbents could be further optimised. To test this hypothesis, we performed an 80-day lab-scale filter experiment and studied As adsorption and oxidation on iron oxide coated sand with scenario modelling.

2. Methods

2.1. Adsorbent

In this research, iron oxide coated sand (IOCS) was used as adsorbent collected from a groundwater-fed rapid sand filter used for drinking water treatment. In this filter, the pH (6.9) and O_2 concentration (3.4 mg/L) are kept low to aim for biological Fe(II) oxidation and to prevent Mn(II)-oxidation. Similar IOCS from drinking water filters are commonly used in full-scale As treatment (Petrusevski et al., 2008, 2007).

2.2. Lab-scale filter design and operation

A PE column with a diameter of 3.3 cm and a height of 1 m was used during the experiment (Fig. 1). IOCS grains were washed and used to fill the column, after which the column was wrapped in aluminium foil. The column was extensively backwashed before the start of the experiment. A salt tracer test was performed in the column to obtain the porosity (=0.28). During the experiment, unchlorinated tap water (for water quality parameter see Appendix 1 (A.1)) was pumped, upflow, into the column (Watson Marlow 300 series, 314D pump head) without any nutrient additions. A small flow of a 15 mg/L As stock was added (Watson Marlow 300 series, 318MC pump head) resulting in a total flow of 146 mL/min, an influent concentration of ~400 μg/L As, a pH between 7.8–8.1, and an O_2 concentration between 9.2–10.0 mg/L. The As stock solution was prepared from a 0.05 M $NaAsO_2$ solution (Merck), and was acidified to about pH 3 by adding 37 % HCl (Fluka) to prevent oxidation during storage, and was refreshed every three days.

2.3. Microbial inhibition procedure

When the As(III) oxidation rate stabilized, the IOCS in the column was flushed with a 25 mM sodium azide (NaN_3, Sigma Aldrich) solution, to inhibit microbial activity. We dosed 500 μg/L As (0.05 M $NaAsO_2$, Merck) to the solution to prevent desorption from the IOCS. The column was saturated with this solution and kept stagnant for 12 h, after which the column was flushed with 15 L for 17 h. ATP measurements were performed before and after microbial inhibition to analyse microbial activity using the Deposit & Surface Analysis kit (LuminUltra Technologies Ltd.) following the protocol provided by the manufacturer. Afterwards, the column was operated identically as at the start of the experiment.

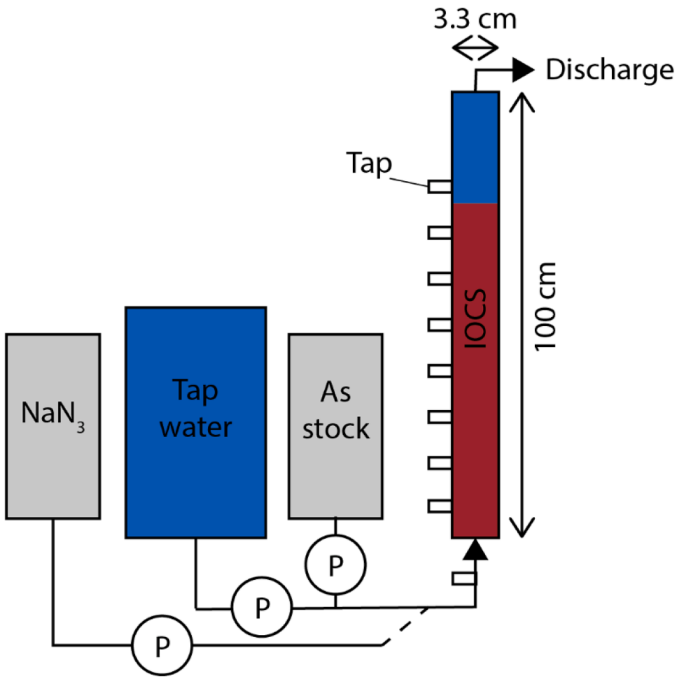

Fig. 1. Schematic overview of the experimental setup, where the P within the circle depict the pumps. During the experiment the column was fed with tap water to which As was added. The tap water and As(III) stock pumps were stopped during microbial inhibition, and only a NaN_3 solution was fed to the column.

2.4. Water sampling and analysis

Water samples were taken periodically from the nine taps on the column (here referred to as height profiles) and more regularly from the influent and effluent water. They were acidified (ROTIPURAN® Ultra 69 %, 1 % v/v) and filtered (0.45 μm) before analysis. Inductively Coupled Plasma Mass Spectrometry (ICP-MS, Analytikal Jena PlasmaQuant MS) was used to determine As(III), As(tot), Fe, and Mn concentrations. The Clifford method was performed to separate As(III) and As(V) using a similar method as described by Gude et al. (2018).

2.5. Characterisation of iron oxide coated sand

IOCS was analysed after collection from the groundwater-fed rapid sand filter. The IOCS coating was extracted following the method proposed by Claff et al. (2010), after which, Fe, Mn and As was analysed using inductively coupled plasma mass spectrometry (ICP-MS, Analytikal Jena Plasma Quant MS). Furthermore, the untouched grain coatings were analysed using light microscopy (VHX-5000 series, Keyence) and Environmental SEM at 0.5 °C and 6 – 8 mbar H_2O atmosphere (Quanta FEG 650, FEI). After the experiments, IOCS grains were collected from close to the influent of the column and analysed using X-ray photoelectron spectroscopy (XPS, for more information see A.2).

2.6. Scenario modelling

The total mass of As adsorbed to the IOCS between two measurement dates was estimated based on the influent and effluent concentrations

and summed for the total period using the following equation,

$$Mass\ adsorbed\ As = \sum (C_{in\_x} - C_{out\_x}) \times (t_x - t_{x-1}) \times q \quad (1)$$

where C_{in_x} is the influent concentration on day x (μg/L), C_{out_x} the effluent concentration on day x (μg/L), t_x is the day since the start of the experiment (days) and t_{x-1} the day since the start of the experiment from the previous measuring round (days), and q is the flow in (L/days).

The exact impact of oxidation and adsorption on the observed concentrations could not be disentangled, which made determining a precise rate of adsorption and oxidation impossible. Instead, two scenarios ("*prevalently As(III)*" or "*prevalently As(V)*", see Table 1) were simulated and compared to the height profiles obtained during the column experiments. We compared the scenarios and used the one that gave the best fit to estimate the rate of adsorption and oxidation in the columns. When no good fits were obtained, As(III) and As(V) concentrations were not simulated. This only occurred when both As(III) and As(V) were present in relatively high concentrations. We presented this data using a third scenario: "*As(III)+As(V)*" (Table 1).

For all scenarios except of *As(III)+As(V)*, sorption was fitted to the As(tot) concentrations, based on a first-order rate equation,

$$As(tot)_{sim} = As(tot)_{in} \times e^{-(k_{sorb} \times t)} \quad (2)$$

where $As(tot)_{sim}$ are the simulated concentrations (μg/L), $As(tot)_{in}$ the influent concentrations (μg/L), k_{sorb} the first order rate constant (s^{-1}), and t the travel time until each tap (s).

Next, biological As(III) oxidation was simulated. Depending on the scenario, we assumed that As(III) (Prevalently As(V); Eq. (3)) or As(V) (Prevalently As(III); Eq. (4)) concentrations were only relying on oxidation (and thus not on adsorption). Lastly, the residual As oxidation state was determined by combining the sorption and oxidation reaction, as As(tot)=As(III)+As(V).

$$\text{Scenario : Prevalently As(V)}\ As(III)_{sim} = As(III)_{in} \times e^{-(k_{ox} \times t)} \quad (3)$$

$$\text{Scenario : Prevalently As(III)}\ As(V)_{sim} = As(V)_{in} + \left(As(III)_{in} \times \left(\left(1 - e^{-(k_{ox} \times t)}\right) + 1\right) - As(III)_{in}\right) \quad (4)$$

3. Results

3.1. Arsenic adsorption

Fig. 2 shows the As concentration in effluent (C_{out}) divided by the influent (C_{in}) during the column experiment (black dots), where a C_{out}/C_{in}=1 means that all As in the influent is also observed in the effluent. The observed trend was similar as seen in prior research (Driehaus et al., 1998; Sperlich et al., 2005). Initially almost all As was adsorbed to the IOCS (C_{out}/C_{in}=0), after which adsorption decreased. The 50 % breakthrough occurred after approximately 15,000 pore volumes and the trend somewhat stabilised after 20,000 pore volumes. Note that still about 25 % of the injected As was adsorbed after more than 70,000 pore volumes, which shows that tailing was still occurring (Fetter et al., 1999). The observed tailing is consistent with recent research into phosphorus adsorption to IOCS, where tailing was found to be caused by slower adsorption on sorption sites in the inner porosity of the iron coating (Barcala et al., 2023). Fig. 2 also shows the cumulative weight of As sorbed to the IOCS (red triangles). Over the course of the experiment, approximately 2080 mg As was sorbed per kg of IOCS in the column (2.08 mgAs/gFe).

Table 1
Scenarios used for fitting to height profiles to estimate oxidation and sorption kinetics.

Scenario name	How is the scenario simulated
Prevalently As (V)	As(V) is prevalently available, thus, we assume that: Only As(V) is sorbed – As(III) concentrations are only depending on oxidation
Prevalently As (III)	As(III) is prevalently available, thus, we assume that: Only As(III) is sorbed – As(V) concentrations are only depending on oxidation
As(III)+As(V)	Simulation is not possible, as both As(III) and As(V) are dominantly available. Therefore, sorption of both solutes is entangled.

3.2. Arsenic speciation in produced water

Fig. 3 shows the As(III) and As(V) concentrations in the effluent during the column experiment. The influent water contained between 211 and 346 μg/L As(III), and between 69 and 151 μg/L As(V). During the first ~5 days of the experiment, As(III) concentrations increased in the effluent water, but always stayed substantially lower than in the influent water. This increase in concentration corresponded to the simultaneous increase in total As concentrations shown in Fig. 2, which was a result of a decrease in sorption capacity. Beyond these initial days, As(III) concentrations stabilised and subsequently decreased after ~12 days. Observed As(V) concentrations increased during this period, indicating a decreasing adsorption capacity of the IOCS. Beyond 12 days, the As(V) concentration in the effluent started to exceed the mean As(V) concentration in the influent. From approximately Day 22, the effluent water only contained As(V) (240 μg/L) and As(III) remained below the detection limit. Clearly, the IOCS column moved towards an almost stable condition where only As(V) was present in the effluent in the course of 20 days.

3.3. Stratification of arsenic oxidation and adsorption

Fig. 4 shows height profiles of the column taken at different days during the experiment. At the start of the experiment (Day 1), As adsorption resulted in a quick decrease of As(tot), As(III), and As(V) over the height of the column. On Day 8, neither As(V) adsorption or production was observed, and As(tot) removal followed the same trend as As(III). From Day 22, As(III) concentrations decreased faster than As (tot) concentrations. At the same time, As(V) concentrations were found to increase over the height of the column. This marks the initiation of As (III) oxidation in the column. On Day 57, As(III) oxidation further accelerated, while As(tot) adsorption remained somewhat stable.

The height profiles were used to estimate the kinetics of As(III) oxidation and As(tot) adsorption using scenario modelling. The scenarios were fitted to the observed concentrations, and the best fitting scenario was used (and shown in Fig. 4) to estimate first order oxidation and sorption rate constants. A good fit was not observed on Day 1; therefore, it was allocated to scenario *As(III)+As(V)*, as likely both As (III) and As(V) sorption occurred. Day 8 was simulated using scenario *Prevalently As(III)*, as oxidation and increasing As(V) concentrations was not observed yet. We assume that biological As(III) oxidation had not yet developed sufficiently this early in the experiment. Furthermore, As(V) adsorption has reached equilibrium, thus all observed removal was due to As(III) adsorption. For Day 22 and 57, As(III) is oxidizing, hence removal occurs primarily through As(V) adsorption, and therefore, scenario *Prevalently As(V)* started to fit best. As(V) sorption became dominant, due to faster As(III) oxidation resulting in higher As(V) concentrations, shifting its earlier adsorption equilibrium.

All days were simulated well using the different scenarios. The first order sorption rate constant (k_{sorb}) decreased over time from 0.012 s^{-1} on day 8 to 0.0035 s^{-1} on day 57. The first order oxidation rate constant (k_{ox}) increased over time from 0 s^{-1} on day 8 to 0.09 s^{-1} on day 57. On day 57, complete As(III) oxidation occurred within <50 s.

3.4. As(V) and As(iii) sorbed to IOCS

Fig. 5A shows a light microscopy image of the IOCS prior to the experiments. The grain coating seemed to be equally distributed over

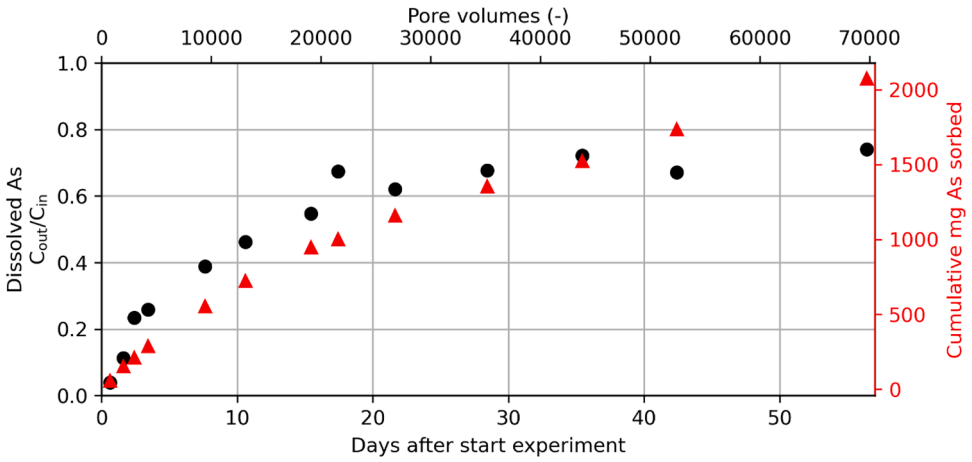

Fig. 2. Fraction of As influent concentrations (C_{in}) divided by effluent concentration (C_{out}) (black dots) and the cumulative weight of As adsorbed to IOCS (red triangles) during the experiment.

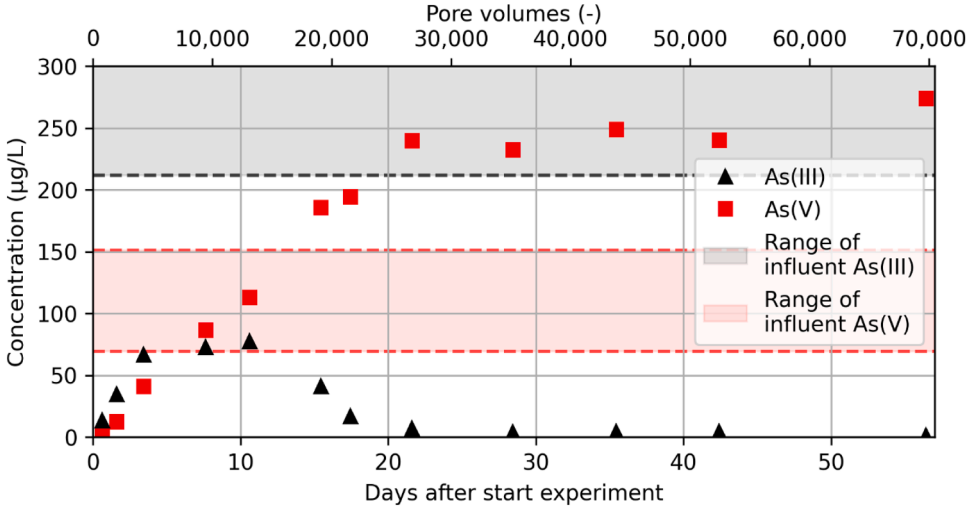

Fig. 3. As(III) (black triangles) and As(V) (red squares) concentrations in effluent water during the first 57 days of the experiment, where the grey and red highlighted background depict the range of influent As(III) and As(V) concentrations, respectively.

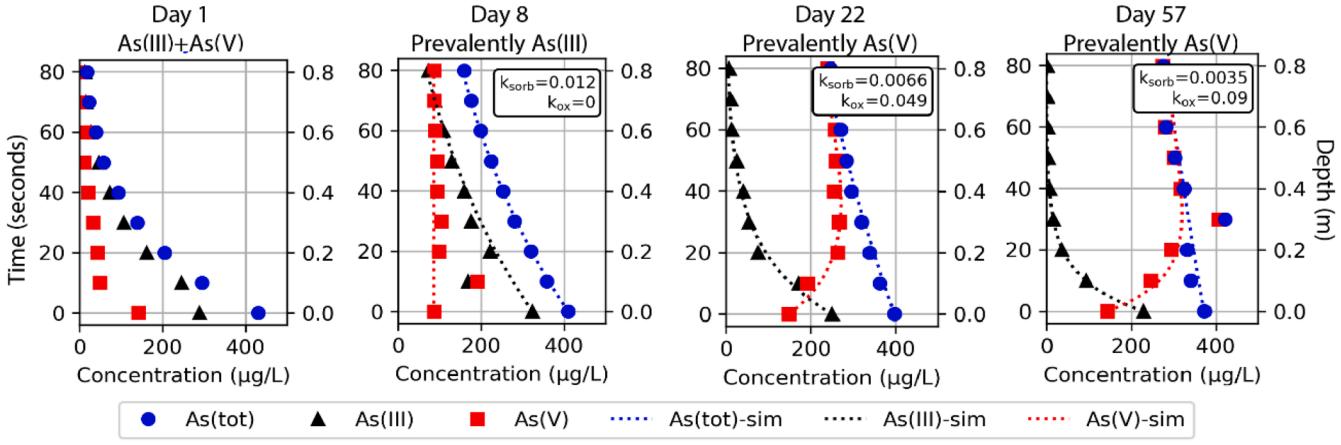

Fig. 4. Height profiles of As(tot), As(III), and As(V) concentrations observed over depth in the IOCS column. The markers (blue circle=As(tot), black triangle=As(III), red square=As(V)) represent the observed concentrations, the dashed lines the simulated scenario fits.

the full surface of the quartz sand grain. The brownish/reddish colour is characteristic for a ferrihydrite coating (Wielinski et al., 2022). Chemical extraction of the coating showed that it contained 440–620 mg/g Fe ($n = 3$) and 0.09–0.12 mg/g Mn ($n = 3$). Furthermore, the grain coating contained 0.16–0.17 ($n = 3$) mg/g As, which corresponds with the relatively high influent As concentrations (~40 µg/L) at the rapid sand

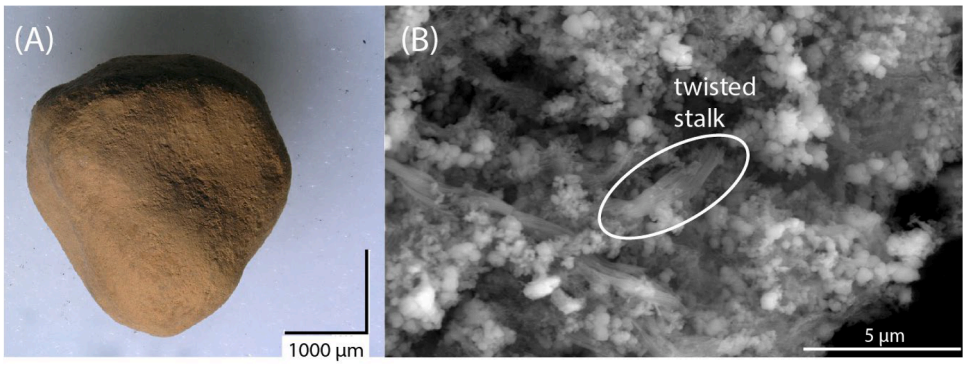

Fig. 5. Images of surface of single IOCS grain taken using a light microscope (A) and ESEM (B).

filter from which the IOCS were obtained. Fig. 5B displays an ESEM image in which the grain coating is 20,000 times magnified. The image shows that the surface of the grain was relatively porous. Furthermore, twisted stalks were observed in the coating, which highlights the biogenic nature of (a part of) the Fe-(hydr)oxides (Chan et al., 2011; Müller et al., 2024).

Grains close to the influent of the column were analysed using XPS for the speciation of the adsorbed As after the experiment. About 53 % As(III) and 47 % As(V) was sorbed to the IOCS (Fig. 6).

3.5. Arsenic oxidation is of biological nature

Microbial activity was inhibited in the column after approximately 50,000 pore flushes, by dosing of NaN_3. A 30-fold reduction of the total ATP, from 29,500–35,100 pg ATP/g ($n = 2$) to 1160–1300 pg ATP/g ($n = 2$), was observed after inhibition. Fig. 7 shows that the effluent water only contained As(V) before microbial inhibition, i.e., all As(III) was oxidized in the column. After microbial inhibition, As(V) concentrations were lower in the effluent and As(III) was observed again. Therefore, oxidation was successfully inhibited, which confirms that oxidation was primarily biological. From Day 9, As(V) concentrations in the effluent water exceeded the mean influent As(V) concentrations. Simultaneously, As(III) concentrations decreased in the effluent, suggesting that biological As(III) oxidation was initiated again. After ~23 days, the effluent primarily contained As(V), which resembles the results prior to microbial inhibition (Fig. 3).

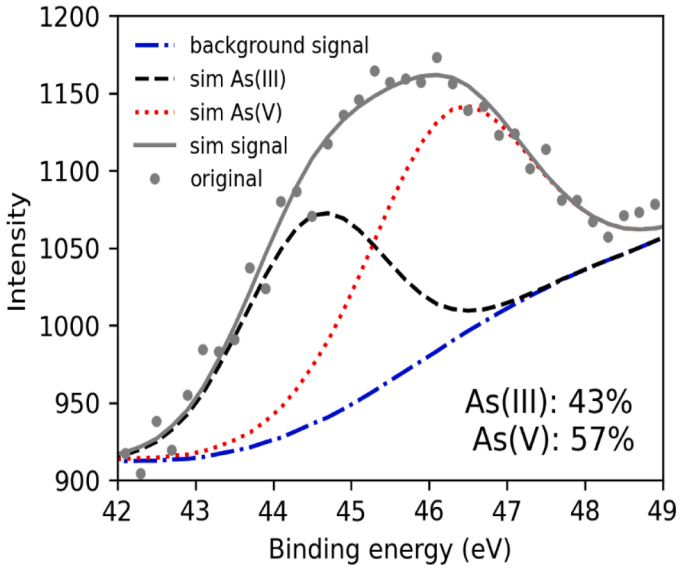

Fig. 6. XPS analysis of As3d spectra of the coating of the grains collected close to the influent of the column.

On Day 1 and Day 2 after microbial inhibition, the height profile was best simulated using scenario *Prevalently As(III),* as oxidation was only limited (k_{ox}=0 and 0.0047, respectively) (Fig. 8). This corresponds to the results of Day 8 prior to inhibition, as no As(V) adsorption is being observed, while As(III) is. The absence of biological oxidation allows for adsorption of As(III), but the consequent lower concentrations of As(V) are not taken up. Once the column ran for a longer period (Day 8 and 16), scenario *Prevalently As(V)* started to fit best, as more As(III) oxidation occurred resulting in higher As(V) concentrations and thus As (V) sorption resumed. This sequence of scenarios is similar to the experiment before microbial inhibition.

The k_{ox} increased over time after microbial inhibition, and followed the same trend and order as before microbial inhibition. A maximum k_{ox} of 0.053 s^{-1} was reached on the last day of the experiment (Day 16), which is in the same order as observed on Day 22 (k_{ox}=0.049 s^{-1}) before microbial inhibition.

4. Discussion

4.1. Biological As(iii) oxidation results in higher adsorption capacity for adsorbent

At the end of the experiment (Day 57), biological As(III) oxidation was fast (k_{ox}= 0.09 s^{-1}). Merely <50 s were needed to fully convert As (III) and As(V) concentrations were higher than As(III) concentrations at almost all depths in the column (Fig. 4). The XPS analysis showed that As (III) and As(V) was somewhat equally adsorbed close to the influent of the column. We expect that the fraction As(III) will only decrease with depth in the column, as (i) at the start almost all As(III) sorption occurred in the upper part of the filter and therefore not much As(III) was adsorbed deeper in the bed, and (ii) later a substantial fraction of As (III) was oxidized to As(V). Consequently, As is primarily adsorbed as As (V), because of its dominant presence and its higher affinity to sorb. This hypothesis is, furthermore, supported by the scenario modelling, and the observed sorption behaviour after microbial inhibition. We did not observe any evidence that As(III) oxidizing biomass masked available adsorption sites on the iron-coated sand. Casentini et al. (2019), similarly, found that arsenic adsorption remained rapid on iron oxide nanoparticles covered with bacterial exopolysaccharide.

Table 2 gives an overview of the operating conditions and performance of three types of full-scale As treatment filters using the Fe-based adsorbents; GEH and IOCS (Driehaus, 2002; Petrusevski et al., 2008, 2007). The life time of the media is considerably longer (0.14–2 years) than the ripening time needed (~weeks) to grow As-oxidizing bacteria observed in the current study and the study of Gude et al. (2018). Furthermore, the contact time (3–120 min) is substantially longer compared to the <50 s needed for complete oxidation observed in the current experiments. Therefore, we deem it likely that biological As(III) oxidation is occurring in these filters, and instead of adsorbing As(III)

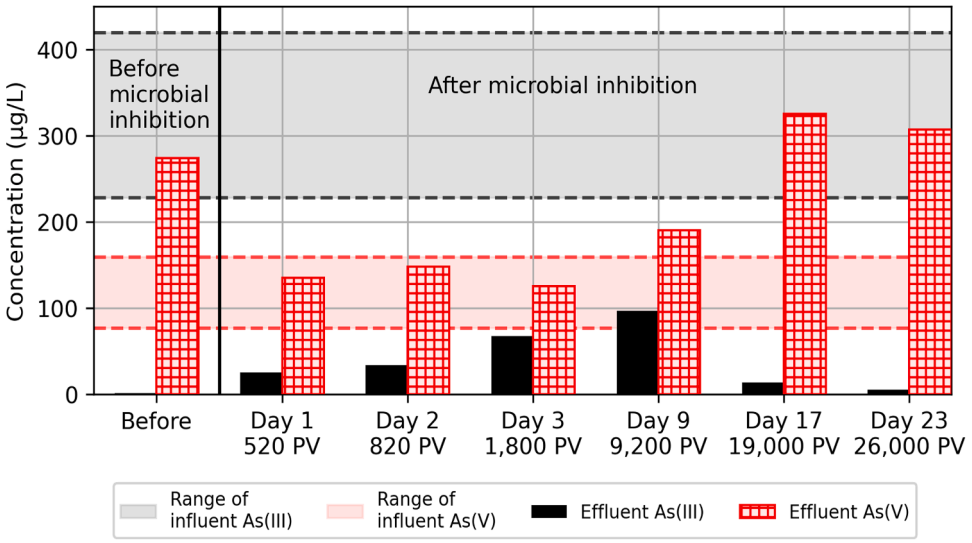

Fig. 7. As(III) (black) and As(V) (red hatched) concentrations in effluent of the column before and after microbial inhibition. The grey and red highlighted background depict the range of influent As(III) and As(V) concentrations, respectively.

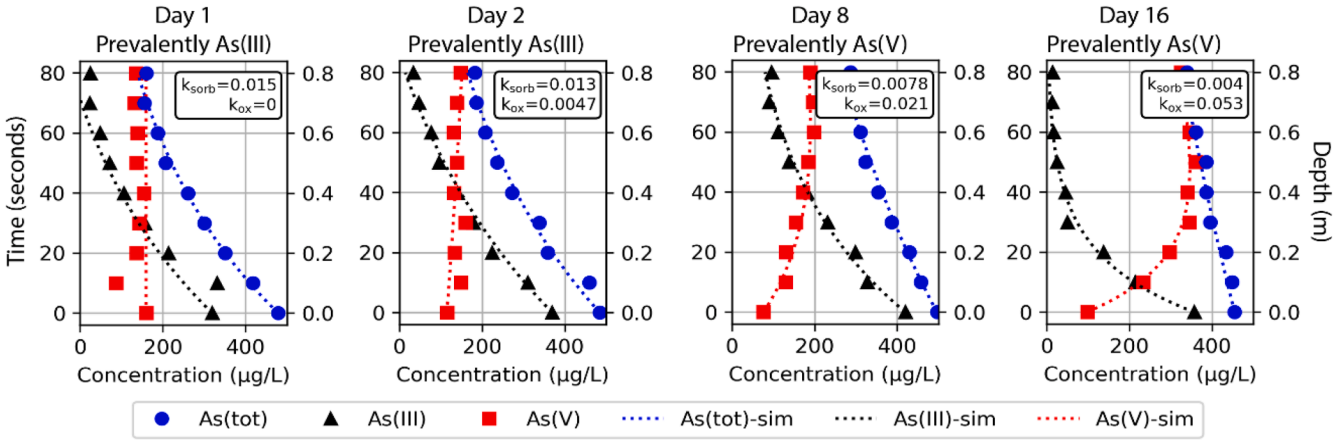

Fig. 8. Height profiles of As concentrations of the IOCS column taken over time after microbial inhibition. The markers (blue circle=As(tot), black triangle=As(III), red square=As(V)) represent the observed concentrations, the dashed lines the simulated scenario fits.

Table 2
Overview of operational conditions of full-scale As treatment plants using iron-based adsorbents.

Operational conditions:	GEH (Driehaus, 2002)	IHE-ADART (Petrusevski et al., 2007)	IHE As removal family filter (Petrusevski et al., 2008)
As in influent water (µg/L)	10–40	20–295	180–480
Flow rates (m^3/h)	4–160	2.3	>0.004
Annual supply (m^3)	10,000–1300,000	~20,000	>36,5
Life time media (years)	~2	>1	0.14 - >2.5
Contact time (min)	3–10 (mean= 4.2 min)	72	120
Treatment capacities (bed volumes)	50,000–200,000	unknown	unknown

the filters are adsorbing As(V). We strongly recommend to study one of the existing As treatment plants based on GEH or IOCS over the height of the filter, in order to assess As(III) oxidation kinetics. When biological As (III) oxidation is observed, the next step for future research would be to identify which bacteria are executing this specific process, and to study the effects of pH, water matrix, and temperature.

Fig. 9 depicts the adsorption capacity trends for a GEH filter where biological As(III) oxidation is occurring (=biotic filter) and not (=abiotic filter). For this analysis, we used the adsorption capacity of As(III) and As(V) on granular ferric hydroxide (GEH) as observed by Driehaus and Dupont (2005). The shown adsorption capacities are a rough estimate, as in the study of Driehaus and Dupont (2005) the influent concentrations are a tenfold lower and GEH is used instead of IOCS. However, note that similar trends for As(III) and As(V) adsorption capacity with pH are also observed for amorphous iron oxides and goethite (Dixit and Hering, 2003), and IOCS (Hsu et al., 2008; Petrusevski et al., 2002). The adsorption capacity in the biotic filter, loaded with As(V), is substantially higher than the abiotic filter loaded with As(III) at a pH below 8. The lower the pH the higher the adsorption capacity in the biotic filter. The adsorption capacity in the abiotic filter is relatively stable from pH 6–9. At pH 6, the adsorption capacity is about an order of magnitude higher for the biotic compared to the abiotic filter. This finding

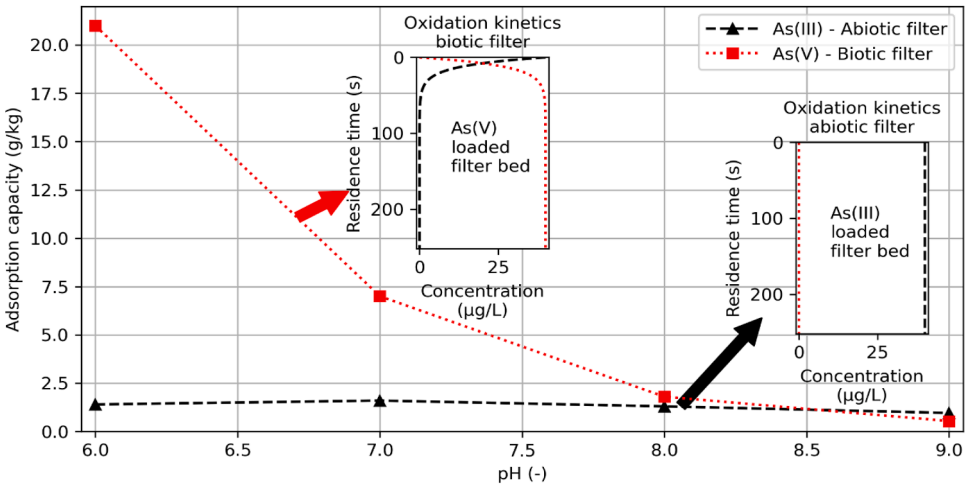

Fig. 9. Adsorption capacity of As(III) as in an abiotic filter and As(V) as in a biotic filter under a range of pH. The oxidation kinetics in the biotic and abiotic filter which regulate As speciation, are appointed with a red and black arrow, respectively. Adsorption capacity is estimated for GEH filters with a mean residence time of 4.2 min, an influent concentration of 40 µg/L, and a first-order oxidation rate constant of 0.09 s^{-1}. For the biotic GEH filter we assumed that only As(V) is present. Adsorption density is based and adapted from Fig. 2 in Driehaus and Dupont (2005).

underlines the value of biological As(III) oxidation in Fe-based adsorbent reactors, as As-free water yields per filter lifetime, i.e., before media replacement, might be up to 10-fold.

4.2. *Leveraging biological As(iii) removal in new filter designs*

The adsorbents in an As treatment plant need to be periodically exchanged, as the adsorbents become exhausted. After the media is exchanged, a ripening period is again needed for the microbiome in the new media to perform biological As(III) oxidation. This ripening period can be eliminated, when the upper layer of the filter, wherein all oxidation occurs, is kept in place. A double-filter system, i.e., two filter tanks in sequence, or a dual media filter, i.e., one tank with two layers of different density, could be suitable to achieve this. In these systems, compartmentalisation of processes can be achieved (Corbera-Rubio et al., 2023). In the case of a dual media bed, this is due to density difference that allow for separation during backwashing. Note that the sorption capacity of the upper layer of the filter will decrease over time until sorption becomes negligible. Therefore, oxidation will occur in the upper layer and sorption in the lower layer. The advantage of the dual media filter is that it takes up a smaller area compared to a double-filter system. For the top layer suitable media should be chosen to host the As (III) oxidizing biofilm, which could be IOCS as in this study, but a lighter material might be more appropriate (e.g., plastic biocarriers, anthracite). The bottom layer has the function to adsorb As(V), so IOCS could be applied, but also activated alumina or ion exchange resins. Frank and Clifford (1986) showed a comparison of an As(III) and an As(V) breakthrough curve of a laboratory experiment using activated alumina. The 50 % breakthrough for As(III) already occurred after 300 pore volumes, while the 50 % breakthrough for As(V) only occurred after 23,400 pore volumes. Similarly, anion exchange is not efficient to treat As(III) (H_3AsO_3), as it can only be applied to remove negatively charged ions. As(V) ($H_2AsO_4^-$ or $HAsO_4^{2-}$) is negatively charged and can be removed by anion exchange (Bissen and Frimmel, 2003). On top of this, exchange resin is interesting because it can easily be regenerated in-situ; maintaining its position below the biological layer. An additional advantage is that the As(V) can be recovered in the regeneration brine, which is of interest, as since 2023, As is on the Critical Raw Materials list of the EU (ENTR, 2023; Wang et al., 2023). This highlights the importance of As as a critical raw material for economic growth, as well as its vulnerability to supply disruptions.

5. Conclusions

This study aimed to investigate the role of biological As(III) oxidation in As removal technologies based on adsorption to iron, e.g., iron oxide coated sand (IOCS), for drinking water production. It was found that As(III) oxidation initiated after approximately 10 days of operating a lab-scale IOCS filter, eventually leading to a first order rate constant of 0.09 s^{-1} after 57 days. Consequently, the initial As(III) adsorbing filter moved towards an As(V) adsorbing filter in ~20 days. After microbial inhibition with NaN_3, As(III) oxidation became negligible, which confirms its biogenic nature. The naturally occurring biological As(III) oxidation, caused by omnipresent bacteria, largely improves the overall performance of filters, as As(V) adsorption capacities tend to be higher than for As(III). We expect that biological As(III) oxidation is also a prevalent process within full-scale As treatment facilities using iron-based adsorbents, as conditions are similar to the performed experiment. These new insights enable further optimization of As treatment using iron based adsorbents. We propose a new reactor design, with a biologically active top layer (i.e., biocarrier) and a bottom layer for the adsorbent. Alternatively, to fully utilise the charge advantage of As(V) at circumneutral pH, an anion exchange resin could be applied to recover As in the brine – since As is recently listed as critical raw material.

CRediT authorship contribution statement

Emiel Kruisdijk: Writing – review & editing, Writing – original draft, Visualization, Validation, Resources, Methodology, Investigation, Formal analysis, Data curation, Conceptualization. **Roos Goedhart:** Writing – review & editing, Methodology, Investigation, Formal analysis, Conceptualization. **Doris van Halem:** Writing – review & editing, Visualization, Validation, Supervision, Project administration, Methodology, Investigation, Funding acquisition, Formal analysis, Data curation, Conceptualization.

Declaration of competing interest

The authors declare that they have no known competing financial interests or personal relationships that could have appeared to influence the work reported in this paper.

Data availability

Data will be made available on request.

Acknowledgements

The authors would like to thank Koen Joris (Pidpa) for providing access to the drinking water treatment plant and the help during sampling, Patricia van den Bos and Jane Erkemeij for their contribution to the laboratory work, and Prasaanth Ravi Anusuyadevi for the XPS analysis. This work was financed by the Netherlands Organisation for Scientific Research (NWO), VIDI project 18369 named: Anoxic-oxic arsenic removal by unravelling redox processes in drinking water filters.

Appendix

A.1. Water quality of influent water

Cl (mg/L)	59
NO_3 (mg/L)	5.6
HCO_3 (mg/L)	120
Na (mg/L)	42
K (mg/L)	6.7
Ca (mg/L)	43
Mg (mg/L)	7.5
Fe (μg/L)	<5
Mn (μg/L)	<5
NH_4 (mg/L)	<0.05
DOC (mg/L C)	2.0

A.2. XPS analysis

The surface chemistry of the particles reported in this manuscript were analysed using X-ray photoelectron spectroscopy (XPS). The grain coating was initially crushed into fine powder using porcelain mortar and pestle. The fine powder was then place on to a 1 × 1 cm2 indium foil substrate. The substrate with the particles to be analysed was subsequently loaded into the PHI-TFA XPS spectrometer (Physical Electronics, Inc. (PHI)), provided with an Aluminium (Al) Kα X-ray monochromatic source (hv = 1486.7 eV).

The vacuum inside the XPS equipment during analysis was maintained around 10–9 mbar. All through the XPS analysis, a circular area of the particle region was analysed with a diameter of 0.4 mm and the depth of analysis was 3 – 5 nm. The pass energy during the full survey study was 89.45 eV with a resolution of 0.5 eV. Followingly, high-resolution multiplex scans of C1s, O1s, Fe2p, Fe3p and Ar3d were performed with a resolution of 0.2 eV, pass energy of 71.55 eV. The take-off angle during both the full survey and high resolution scans was at 45o.

All the obtained spectra using the XPS machine were processed using the MultiPak version 8.0 software provided by Physical Electronics Inc. In order to compensate the charging of the samples during the XPS analysis, prior to curve fitting of the XPS data, all the spectra were adjusted by doing the carbon shift, C—C peak of C1s spectrum was set at 284.4 eV.

The As(III) binding energy peak was observed at 44.5 eV, and for As(V) at 46.2 eV. These binding energies correspond to the range of 44.3–44.5 and 45.2–46.2 reported in previous studies (Fullston et al., 1999; Han et al., 2011; Nesbitt et al., 1998; Viltres et al., 2020). The percentage availability of As(III)/As(V) was determined based on the area of the peaks.

References

Banerjee, K., Amy, G.L., Prevost, M., Nour, S., Jekel, M., Gallagher, P.M., Blumenschein, C.D., 2008. Kinetic and thermodynamic aspects of adsorption of arsenic onto granular ferric hydroxide (GFH). Water Res. 42, 3371–3378.

Barcala, V., Zech, A., Osté, L., Behrends, T., 2023. Transport-limited kinetics of phosphate retention on iron-coated sand and practical implications. J. Contam. Hydrol. 255, 104160.

Bissen, M., Frimmel, F.H., 2003. Arsenic — A review. Part II: oxidation of arsenic and its removal in water treatment. Acta Hydroch. Hydrob. 31, 97–107.

Casentini, B., Gallo, M., Baldi, F., 2019. Arsenate and arsenite removal from contaminated water by iron oxides nanoparticles formed inside a bacterial exopolysaccharide. J. Environ. Chem. Eng. 7, 102908.

Chan, C.S., Fakra, S.C., Emerson, D., Fleming, E.J., Edwards, K.J., 2011. Lithotrophic iron-oxidizing bacteria produce organic stalks to control mineral growth: implications for biosignature formation. ISME J. 5, 717–727.

Claff, S.R., Sullivan, L.A., Burton, E.D., Bush, R.T., 2010. A sequential extraction procedure for acid sulfate soils: partitioning of iron. Geoderma 155, 224–230.

Corbera-Rubio, F., Laureni, M., Koudijs, N., Müller, S., van Alen, T., Schoonenberg, F., Lücker, S., Pabst, M., van Loosdrecht, M.C.M., van Halem, D., 2023. Meta-omics profiling of full-scale groundwater rapid sand filters explains stratification of iron, ammonium and manganese removals. Water Res 233, 119805.

Crognale, S., Amalfitano, S., Casentini, B., Fazi, S., Petruccioli, M., Rossetti, S., 2017. Arsenic-related microorganisms in groundwater: a review on distribution, metabolic activities and potential use in arsenic removal processes. Rev. Environ. Sci. Bio/Technol. 16, 647–665.

Crognale, S., Casentini, B., Amalfitano, S., Fazi, S., Petruccioli, M., Rossetti, S., 2019. Biological As(III) oxidation in biofilters by using native groundwater microorganisms. Sci. Total Environ. 651, 93–102.

Dixit, S., Hering, J.G., 2003. Comparison of arsenic(V) and arsenic(III) sorption onto iron oxide minerals: implications for arsenic mobility. Environ. Sci. Technol. 37, 4182–4189.

Driehaus, W., 2002. Arsenic removal - experience with the GEH® process in Germany. Water Supply 2, 275–280.

Driehaus, W., Dupont, F., 2005. Arsenic removal-solutions for a world wide health problem using iron based adsorbents. J. Europeen D Hydrologie 36, 119.

Driehaus, W., Jekel, M., Hildebrandt, U., 1998. Granular ferric hydroxide—A new adsorbent for the removal of arsenic from natural water. J. Water Supply: Res. Technol.-Aqua 47, 30–35.

ENTR, 2023. Study On the Critical Raw Materials For the EU 2023 – Final report. Publications Office of the European Union.

Fetter, C.W., Boving, T.B., Kreamer, D.K., 1999. Contaminant Hydrogeology. Prentice hall Upper Saddle River, NJ.

Frank, P., Clifford, D.A., 1986. Arsenic (III) Oxidation and Removal from Drinking Water. Water Engineering Research Laboratory, Office of Research and Development, US Environmental Protection Agency.

Fullston, D., Fornasiero, D., Ralston, J., 1999. Oxidation of synthetic and natural samples of enargite and tennantite: 2. X-ray photoelectron spectroscopic study. Langmuir 15, 4530–4536.

Gude, J.C.J., Rietveld, L.C., van Halem, D., 2018. Biological As(III) oxidation in rapid sand filters. J. Water Process Eng. 21, 107–115.

Gupta, V.K., Saini, V.K., Jain, N., 2005. Adsorption of As(III) from aqueous solutions by iron oxide-coated sand. J. Colloid Interface Sci. 288, 55–60.

Han, X., Li, Y.-L., Gu, J.-D., 2011. Oxidation of As(III) by MnO2 in the absence and presence of Fe(II) under acidic conditions. Geochim. Cosmochim. Acta 75, 368–379.

Hao, L., Liu, M., Wang, N., Li, G., 2018. A critical review on arsenic removal from water using iron-based adsorbents. RSC Adv. 8, 39545–39560.

Hsu, J.C., Lin, C.J., Liao, C.H., Chen, S.T., 2008. Removal of As(V) and As(III) by reclaimed iron-oxide coated sands. J. Hazard. Mater. 153, 817–826.

IARC, 2004. International agency for research on cancer working group on the evaluation of carcinogenic risks to humans world health organization: some drinking-water disinfectants and contaminants, including arsenic. IARC.
Kamei-Ishikawa, N., Segawa, N., Yamazaki, D., Ito, A., Umita, T., 2017. Arsenic removal from arsenic-contaminated water by biological arsenite oxidation and chemical ferrous iron oxidation using a down-flow hanging sponge reactor. Water Supply 17, 1249–1259.
Kim, M.-J., Nriagu, J., 2000. Oxidation of arsenite in groundwater using ozone and oxygen. Sci. Total Environ. 247, 71–79.
Li, H., Zeng, X.-C., He, Z., Chen, X., E, G., Han, Y., Wang, Y., 2016. Long-term performance of rapid oxidation of arsenite in simulated groundwater using a population of arsenite-oxidizing microorganisms in a bioreactor. Water Res. 101, 393–401.
Mähler, J., Persson, I., 2013. Rapid adsorption of arsenic from aqueous solution by ferrihydrite-coated sand and granular ferric hydroxide. Appl. Geochem. 37, 179–189.
Miklos, D.B., Remy, C., Jekel, M., Linden, K.G., Drewes, J.E., Hübner, U., 2018. Evaluation of advanced oxidation processes for water and wastewater treatment – A critical review. Water Res. 139, 118–131.
Mohan, D., Pittman, C.U., 2007. Arsenic removal from water/wastewater using adsorbents—A critical review. J. Hazard. Mater. 142, 1–53.
Müller, S., Corbera-Rubio, F., Schoonenberg-Kegel, F., Laureni, M., Loosdrecht, M.C.M. v., Halem, D.v., 2024. Shifting to biology promotes highly efficient iron removal in groundwater filters. Biorxiv, 2024.2002.2014.580244.
Nesbitt, H.W., Canning, G.W., Bancroft, G.M., 1998. XPS study of reductive dissolution of 7Å-birnessite by H3AsO3, with constraints on reaction mechanism. Geochim. Cosmochim. Acta 62, 2097–2110.
Petrusevski, B., Boere, J., Shahidullah, S.M., Sharma, S.K., Schippers, J.C., 2002. Adsorbent-based point-of-use system for arsenic removal in rural areas. Journal of Water Supply: Research and Technology-Aqua 51, 135–144.
Petrusevski, B., Sharma, S., van der Meer, W.G., Kruis, F., Khan, M., Barua, M., Schippers, J.C., 2008. Four years of development and field-testing of IHE arsenic removal family filter in rural Bangladesh. Water Sci. Technol. 58, 53–58.
Petrusevski, B., van der Meer, W., Baker, J., Kruis, F., Sharma, S.K., Schippers, J.C., 2007. Innovative approach for treatment of arsenic contaminated groundwater in Central Europe. Water Supply 7, 131–138.
Podgorski, J., Berg, M., 2020. Global threat of arsenic in groundwater. Science 368, 845–850.
Siddiqui, S.I., Chaudhry, S.A., 2017. Iron oxide and its modified forms as an adsorbent for arsenic removal: a comprehensive recent advancement. Process Saf. Environ. Prot. 111, 592–626.
Sperlich, A., Werner, A., Genz, A., Amy, G., Worch, E., Jekel, M., 2005. Breakthrough behavior of granular ferric hydroxide (GFH) fixed-bed adsorption filters: modeling and experimental approaches. Water Res. 39, 1190–1198.
Thirunavukkarasu, O.S., Viraraghavan, T., Subramanian, K.S., 2003. Arsenic removal from drinking water using iron oxide-coated sand. Water Air Soil Pollut. 142, 95–111.
Viltres, H., Odio, O.F., Lartundo-Rojas, L., Reguera, E., 2020. Degradation study of arsenic oxides under XPS measurements. Appl. Surf. Sci. 511, 145606.
Wan, J., Klein, J., Simon, S., Joulian, C., Dictor, M.-C., Deluchat, V., Dagot, C., 2010. AsIII oxidation by Thiomonas arsenivorans in up-flow fixed-bed reactors coupled to As sequestration onto zero-valent iron-coated sand. Water Res. 44, 5098–5108.
Wang, K., Holm, P.E., Trettenes, U.B., Bandaru, S.R.S., van Halem, D., van Genuchten, C. M., 2023. Molecular-scale characterization of groundwater treatment sludge from around the world: implications for potential arsenic recovery. Water Res. 245, 120561.
Weerasundara, L., Ok, Y.-S., Bundschuh, J., 2021. Selective removal of arsenic in water: a critical review. Environ. Pollut. 268, 115668.
WHO, 1993. Guidelines for drinking-water quality. World Health Organization.
Wielinski, J., Jimenez-Martinez, J., Göttlicher, J., Steininger, R., Mangold, S., Hug, S.J., Berg, M., Voegelin, A., 2022. Spatiotemporal mineral phase evolution and arsenic retention in microfluidic models of zerovalent iron-based water treatment. Environ. Sci. Technol. 56, 13696–13708.